SINERGI Vol. 26, No. 2, June 2022: 237-248
http://publikasi.mercubuana.ac.id/index.php/sinergi
http://doi.org/10.22441/sinergi.2022.2.013

Effect of forging load and heat treatment process on the corrosion behavior of A588-1%NI for weathering steel application in a marine environment

Miftakhur Rohmah*, Permana Andi Paristiawan, Toni B. Romijarso
Research Center for Metallurgy and Materials, National Research and Innovation Agency (BRIN), Indonesia

Abstract
The study focused on the effect of forging load and heat treatment on the corrosion behavior of A588-1%Ni weathered steel. The samples used were hot forged steel (A588%-1%Ni) with a load of 50 tons and 75 tons at a temperature of 800-850 °C. The test sample was reheated at an intercritical temperature between A_3–A_1, around 780 °C, held for 1 hour, and then cooled to room temperature. The cooling media used are water, oil, and open air. Forging loads and heat treatment variation affect the microstructure and corrosion rate of A588-1%Ni. Based on the metallographic test and after the hot forging process, A588-1%Ni laterite steel has a microstructure as ferrite-perlite. Then, after heat treatment as ferrite and cementite-containing phase, pearlite, bainite, or martensite may very well. Cooling water delivers a uniformly distributed lath martensite with an acicular ferrite phase. In addition, the oil media creates bainite with an acicular ferrite phase coarser size. The open-air media produces a pearlite + ferrite phase. Corrosion behavior of laterite steel subjected to hot forging process and followed by heat treatment was evaluated in 3% NaCl solution. Oil cooling with bainite-ferrite microstructure has the lowest corrosion rate, which is 11.96x10^{-3} mmpy.

Keywords:
A588-1%;
Cooling Media;
Hot Forging;
Weather Resistant Steel;

Article History:
Received: September 22, 2021
Revised: December 21, 2021
Accepted: December 26, 2021
Published: June 15, 2022

Corresponding Author:
Miftakhur Rohmah
Research Center for Metallurgy and Materials, National Research and Innovation Agency, Indonesia
Email:
miftakhur.rohmah@brin.go.id

INTRODUCTION

In the marine environment, weathering steel (or Corten Steel) in the bridge construction structure is viewed as one of the steps to reduce maintenance costs, especially adding paint. The Corten Steel would form a protective rust layer and hinder severe corrosion in an environment with high salinity [1]. The corrosivity of marine is due to salinity salt (mainly NaCl). The seawater salinity varies from around 3% to 3.6%, at an average of 3.5% [2][3]. Therefore, an important class of bolted alloys must have high toughness and be able to consistently resist corrosion-erosion caused by climate changes to extend the product's service life. As of late, low-alloy steels have developed into high-strength and high-hardness steels. Corten Steel is a high-low strength alloy with limited quantities of Cu, Cr, Ni, and P, which is detailed to form a defensive patina layer. The total alloy content is around 1-5% mass, which is higher than low carbon steels [4]. However, Corten A588 Steel likewise has a moderately low strength of 435-485 Mpa [5], thus improving mechanical properties and formability. Consequently, this research focuses on using lateritic steel as an alternative material to manufacture A588 Corten Steel.

Nickel metal-containing laterite is an important source of early nickel minerals, further converted and processed into high-strength special steels with good corrosion resistance and great weldability. Nickel stabilizes steel's austenitic structure at room temperature with an austenitic structure (FCC crystal) is a very strong and ductile [6]. A-588

has a ferrite-perlite microstructure with fine grain size due to rolling or heat treatment [5]. In the development of laterite steel, open die forging is mainly used to produce large parts requiring high mechanical properties and reliability with efficient manufacturing economic. Satrio et al. expressed that hot forging with forging load variations of 500, 750, and 1000 kN in open die forging caused grain refinement of the ferrite-perlite microstructure due to the grain recrystallization mechanism, accordingly increasing the hardness and impact resistance [7]. Hasbi et al. used a 100-ton forging process followed by a heat treatment process-water and oil cooling medium to form a ferrite-martensite double-phase structure, subsequently improving the hardness and toughness Fe-Ni steel [8]. There is still very limited information on the characteristics of lateritic steel resulting from the forging process followed by heat treatment for the application of Corten Steel. Laterite steel is one alternative for national steel production independently to reduce imports of high-strength steel which is needed for infrastructure development in Indonesia [6]. The forging result in steel is stronger than cast or machined metal parts. Achieve the requirements in terms of a good amount of deformation in lateritic steel forging is related to eliminating any porosity in the material and refining the grain size. So, the 50 and 75 ton load is used in the hot forging process. When the temperature of forging steel is above about 2200 °F, the reduction of at least 15-20% and refined grain size is required. An optimized process gives a good quality forging with minimum load [9]. The forging machine can apply the 50 and 75 ton minimum forged.

Steel microstructure plays a major role in pitting corrosion propagation, affecting its corrosion resistance. When Corten Steel contains two or more phases, micro-galvanic corrosion is possible. Zhang et al. analyzed the effect of steel microstructure using electrochemical-potentiodynamic methods. In 0.1 M NaCl media, the order of corrosion potential value is $Ecorr_{(ferrite)} > Ecorr_{(bainite)} > Ecorr_{(perlite)}$, and the corrosion current density value is $Icorr_{(ferrite)} < Icorr_{(bainite)} < Icorr_{(perlite)}$ [10]. The pearlite phase consists of ferrite+cementite (Fe_3C), while the bainite granular phase consists of bainite ferrite and martensite islands. Wang et al. observed that the content of ferrite + pearlite phase and bainite ferrite + martensite island-austenite residual phase would accelerate corrosion propagation in 0.5 wt% NaCl media. The spatial distribution of bainite is more homogeneous than pearlite. Therefore, bainite shows a more stable electrochemical activity [11]. Hao et al. observed the formation of micro-galvanic pairing between the lamellar cementite phase and ferrite phase, which increases the corrosion rate of ferrite-perlite steel in hydrochloric acid solution. The anodic dissolution of the ferrite phase is regulated by the charge transfer process, while the cathodic reaction of the cementite phase is regulated by the diffusion process [12]. Corrosion of atmospheric exposed Corten Steels is affected by incorporating microstructures with varying degrees of electrochemical activity.

The composition of the alloy and the difference in heat, chemical, or mechanical treatment determined the mechanical properties of Corten Steel. Therefore, research on the effect of thermomechanical processes on the corrosion behavior of weather-resistant steels in the marine environment is very important for designing the A588-1%Ni composition. The research focuses on combining the hot forging process and heat treatment of A588-1%Ni laterite steel in microstructure and its effect on corrosion resistance. The average salinity of the sea is 3.5%

METHOD

Instrumentation

The instrumentation used consists of the induction furnace melting (Inductotherm brand butterfly type) with a 100kg-capacity, Optical Emission Spectroscopy (OES) Bruker Q4 Tasman, forging machine brand Liyaoyang Metal Forming Type J53, muffle furnace, Olympus BX-53M optical microscope, Micro-vickers Hardness Test, Gamry G-750 system, saturated calomel electrode, and platinum electrode

Material

Modification of casted laterite steel (A588-1% Ni) is used as material in this research. The chemical composition of the modified A588 laterite steel with 1% nickel is shown in Table 1. Furthermore, the manufacture of the test sample from the starting material was carried out by a milling process so that the final dimensions of the test sample were Ø20cm and 20cm high, with both surfaces flattened.

Hot Forging and Heat Treatment Process

Eight pieces of A588-1%Ni Laterite Steel were prepared to be a test sample in the hot forging process with a size of Ø 20 cm and a height of 20 cm.

Table 1. Chemical composition of A-588 laterite steel

Component (%mass)	Materials	
	ASTM A-588	Modified of A588-1%Ni
C	0.17 maks	0.17
Mn	0.50-1,2	0.48
Cr	0.4-0,7	0.68
Mo	0.1 maks	0.03
Ni	0.4 maks	1.13
P	0.04 maks	0.04
Si	0.25-0,5	0.32
S	0.05 maks	0.03
Fe	*Balance*	*Balance*

The test sample was subjected to a hot forging process with variations in the compressive load of (a) 50 and (b) 75 tons to determine the effect of the forging load. The test sample was heated at a temperature of 950 °C for 1 hour, and then subjected to an open die forging process - 1x loading cycle. After the forging process, a heat treatment process is applied to determine the transformation of the double phase structure. The test sample was reheated at a temperature between A_3–A_1, about 780 (C), held for 1 hour, and then cooled to room temperature. The approximate temperatures A_3 and A_1 for this sample are 874 °C and 746 °C, according to (1) and (2) [13]. The cooling media used are water, oil, and open air. The sample was coded to simplify the process, as described in Table 2.

$$A_1 = 751 - 16.3(\%C) - 27.5(\%Mn) - 5.5(\%Cu) - 5.9(\%Ni) + 34.9(\%Si) + 12.7(\%Cr) + 3.4(\%Mo) \quad (1)$$

$$A_3 = 881 - 20.6(\%C) - 15(\%Mn) - 26.5(\%Cu) - 20.1(\%Ni) + 53.1(\%Si) + 12.7(\%Cr) + 41.7(\%V) \quad (2)$$

Metallographic and Hardness Test

Metallographic testing was carried out using an Olympus BX-53M optical microscope. The test sample was cut into 1x1 cm sizes.

Table 2. Sample test description

Code	Description
1A	Hot Forged 50 ton
2A	Hot Forged 75 ton
1B	Hot Forged 50 ton + Heat Treatment (water cooling)
2B	Hot Forged 75 ton + Heat Treatment (Water Cooling)
1C	Hot Forged 50 ton + Heat Treatment (oil cooling)
2C	Hot Forged 75 ton + Heat Treatment (oil cooling)
1D	Hot Forged 50 ton + Heat Treatment (open-air cooling)
2D	Hot Forged 75 ton + Heat Treatment (open-air cooling)

Then, it is mounted using epoxy resin, and sanded with SiC starting from 80, 100, 200, 600, 800, 1000, 1200 sequentially up to 2000 grids, and polished with an alumina paste that was given a size 1, 0.5, and 0.3µm, so that the surface of the test sample is shiny without a scratch. The etching solution used is nital 2%. The hardness test was carried out using Micro-Vickers Tester with 5N for 10s indentation load.

Corrosion Test

The test sample was cut into 1x1 cm and then soldered with copper wire until electrical contact occurred. Next, the samples were mounted using epoxy resin and sanded with SiC paper ranging from 80-800 grit. Next, corrosion testing was carried out using the Tafel-polarization method using the Gamry G-750 system.

The sample as the working electrode was connected in a circuit with a reference electrode (saturated calomel electrode) and an auxiliary electrode (platinum) during the test process. Before testing, the open circuit potential or OCP (E_{oc}) was measured for 3600 seconds. Then, the polarization test was carried out at a potential range of -200mV to +200 mV with a scan speed of 1mV/s in a 3% NaCl solution. 3% NaCl prepared from distilled water is used as commonly artificial seawater for corrosion in the marine environment [14].

RESULTS AND DISCUSSION

CCT Diagram Simulation

The CCT Diagram of weathering steel A588-1% Ni is simulated using JmatPro® and shown in Figure 1. The CCT confirms the relationship between continuous cooling rate and microstructure.

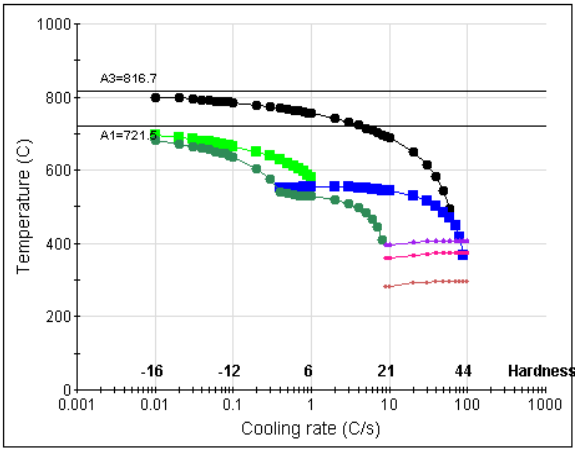

Figure 1. CCT Diagram of A588-1% (black = ferrite, dark green = austenit, light green = pearlite, blue = bainite, and violet = martensite)

Based on Figure 1, the Ac1 and Ac3 are 721 °C and 816.7 °C, so the temperature of 780 °C used in this work is the intercritical temperature between Ac1 and Ac3. The Bainite start (Bs) temperature is almost 580 °C and the martensite start (Ms) temperature is 400 °C. Under the experiment (cooling rate around 5 °C/s for open-air cooling, 20 °C /s for oil cooling, and 25 °C /s for water cooling), there is bainite transformation included for all samples. The change in cooling rate greatly affects the decomposition kinetics of metastable austenite during continuous cooling [15].

Microstructure and Hardness Analysis

Metallographic testing is carried out to determine the final microstructure to predict the phase transformations that occur during the hot forging and heat treatment processes. The microstructure of as-cast Fe-Ni steel with the same chemical composition is ferrite and pearlite [8]. The microstructure of Laterite A588-1%Ni steel after hot forging followed by heat treatment is shown in Figure 2 and Figure 3. In this study, the final temperature in the hot forging process is close to the equilibrium temperature of the austenite to ferrite transition, which is 800-850 ℃.

Based on Figure 2, the microstructure of A588 laterite steel after the hot forging process consists of ferrite and pearlite. The ferrite is indicated by light colour, while the pearlite is a dark colour. The forging process does change the size and shape of the grains. Loading of 50 tons (sample 1A) resulted in ferrite with an elongated shape (irregular columnar), while loading of 75 tons (sample 1B) caused ferrite with an irregular block shape. It is in line with Zhang et al., who stated that pearlite in forged steels is distributed mainly in the shear band, and pearlite is deformed in the direction of growth [16]. In addition, the loading of 75 tons tends to have a smaller ferrite grain size when compared to the loading of 50 tons. The estimate of average grain size is performed in ASTM E112 with Heyne Lineal Intercept Procedure. The 50-ton load is produced standard grain size of ASTM G number 15 ($6.554x10^6$ grain/mm^2), and the 75-ton load is produced standard grain size of ASTM G number 15.6 ($9.933\ x10^6$ grain/mm^2). Thus, the greater the forging load, the smaller the grain size formed. This grain size can be attributed to the fact that grain flow growth tends to be suppressed by some of the defects created during forging and the nickel content affects the formation of the amount of austenite upon heating. The forging load is correlated with the degree of thickness reduction of the geometry sample. The forging process with a load of 50 tons resulted in an 18±0.2% reduction, and 75 tons resulted in a 31±1% reduction.

In addition, heat treatment changes the microstructure of the A588 laterite steel shown in Figure 3. The forging process followed by heat treatment will be associated with recrystallization and growth of austenite grains. Figure 3 shows the transformation of the microstructure after being subjected to intercritical heating with various cooling media.

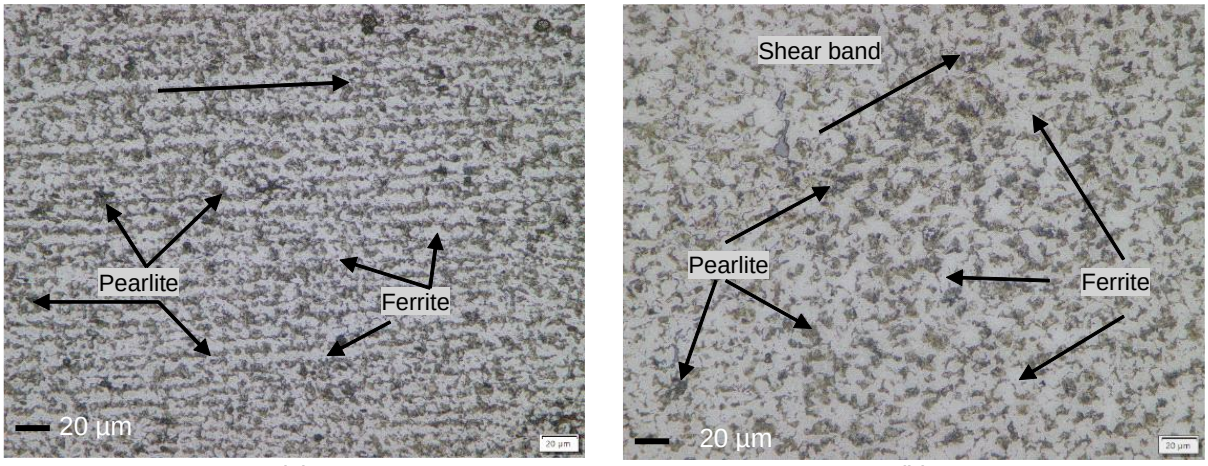

(a) (b)

Figure 2. Microstructure of A588-1%Ni laterite steel after hot forging without heat treatment (a) 75-ton and (b) 50 ton

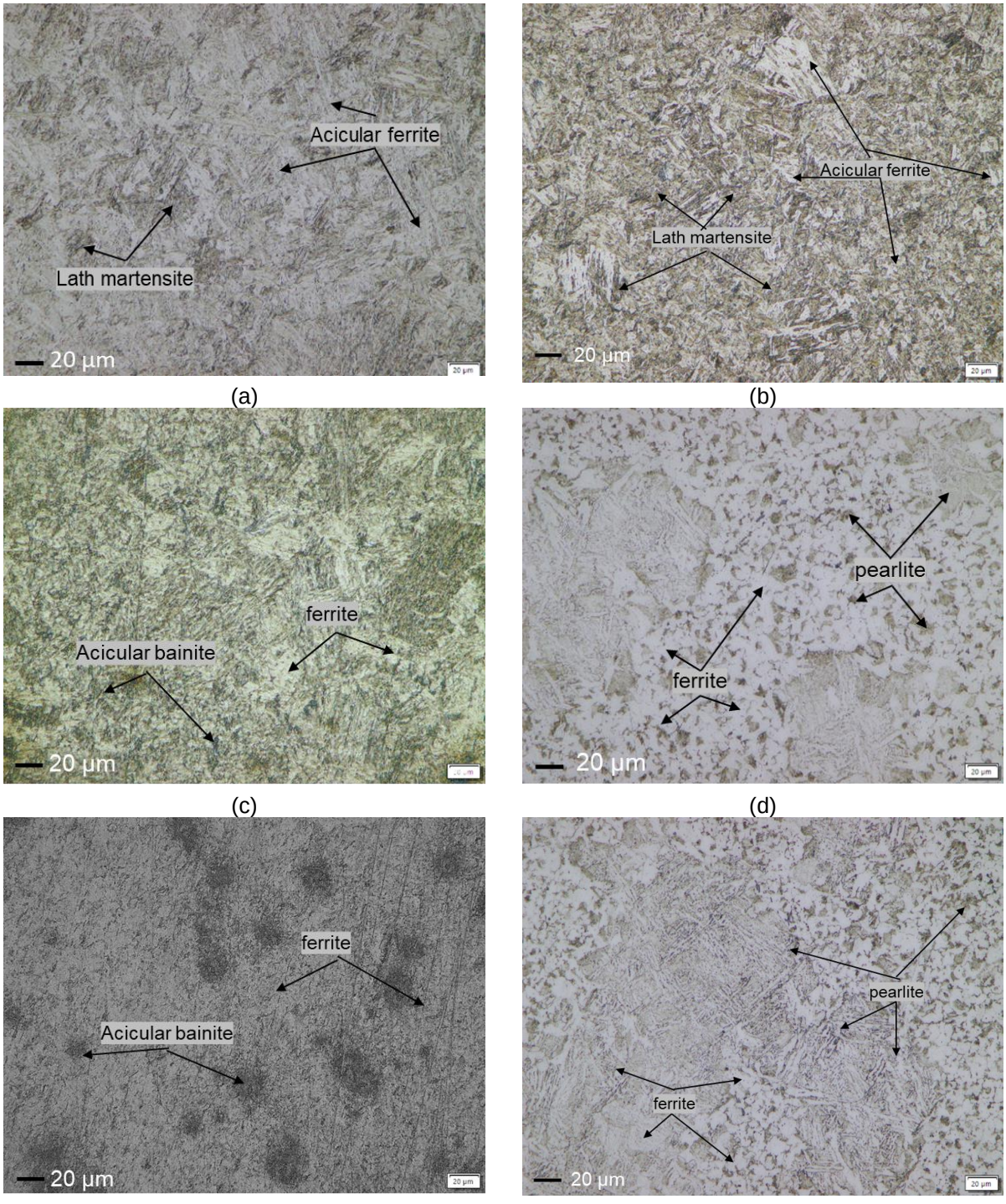

Figure 3. Microstructure of A588-1%Ni after hot forging and followed by heat treatment (a) 50 ton (b) 75 ton water cooling (c) 50 ton (d) 75 ton oil cooling (e) 50 ton (f) 75 ton open-air cooling

In general, the microstructure of A588-1%Ni laterite steel after heat treatment is ferrite and a phase containing cementite, which can be pearlite, bainite, or martensite, which tends to be difficult to distinguish with optical microscope resolution. Figure 3a-3b shows samples 1B and 2B dominated by the lath martensite + acicular ferrite phase, evenly distributed. Acicular ferrite transformation implies needle morphology or highly structured non-equiaxed ferrite, generally applied to groups of ferrite plates or lath and more likely to happen at low temperature as a

diffusionless reaction [15][17]. Figure 3c-3d shows samples 1C and 2C dominated by acicular bainite + ferrite. Shao et al. suggest that the higher cooling rate promotes acicular ferrite and bainite transformation and delays polygonal ferrite and pearlite formation [15]. In addition, Figure 3e-3f shows samples 4A and 4B dominated by the pearlite with ferrite phase. Ferrite is only formed with a cooling rate of 0.1–100 °C/s in lateritic steel with 1% nickel [18]. Acicular ferrite grows by a shear diffusionless mechanism similar to bainite, wherein ferrite grows without diffusion and becomes saturated in carbon [15][19]. Shear diffusionless lead to a small displacement of atoms in the structure, like a martensitic transformation. The structure may result from the carbon partitioning near the austenite/ferrite interface during cooling conditions [20]. Water cooling media provides a fast-cooling rate and does not allow the carbon contained in austenite (FCC) to diffuse into ferrite (BCC); Austenite will be transformed into a metastable phase of martensite and bainite [8].

The size of the martensite lath was gradually refined with an increase in cooling rate of 10-40 °C/s so that many entangled dislocations were distributed within the martensite lath boundary [21]. Rapid cooling rates (aqueous medium or exceeding 10 ℃/s) tend to produce martensite lath, while fairly fast cooling rates (oil media) allow the transformation of lower bainite or martensite to larger/coarse sizes. Austenite decomposition forms bainite at temperatures above the martensite formation temperature (Ms) but below the pearlite formation transformation temperature, around 250-500 ℃. This is because the upper bainite has an austenite film retained in the ferrite without the martensite-austenite constituent [22].

Heat treatment with air media (otherwise known as normalizing) forms microstructures in polygonal ferrite, lamellar pearlite, and lower bainite. Polygonal ferrite in bainite is obtained with a cooling rate between 0.05-1 °C/s uneven loading of the forging so that there are recrystallized and non-recrystallized areas. The absence of martensite lath due to the slow cooling rate allows sufficient time for the austenite to transform to pearlite.

SEM Micrographs of A588-1% to observe the microstructure in clear detail are shown in Figure 4. Figure 4 shows significant morphological differences due to differences in cooling rates. In Figure 4(a), the morphology consists of irregular - needle shapes indicated as ferrite and lath martensite. In comparison, Figure 4(b) consists of block morphology like an island and is indicated as bainite. Figure 4(c) shows an irregular plate as pearlite and a matrix as ferrite. The microstructure characteristics of acicular ferrite are similar to bainite, so this phase is classified as a bainitic transformation product [17]. A higher cooling-rate increases supercooling and driving force reaction, leading to a higher nucleation rate and acicular ferrite plates nucleating. Ni, Mn, Cr, and Mo act as a solute and positively affect the formation of acicular ferrite at low content [19]. The elemental in each phase is shown in Table 3.

According to Table 3, the solute atoms such as Cr, Mn, and Ni dissolved in the iron matrix can accumulate in the grain boundary and become for corrosion preferential initiation [23].

The strength and hardness are primarily controlled by the alloy chemistry and the heat treatment given to the forging. For example, the hardness of A588-1% Ni is depicted in Figure 5.

According to Figure 5 and Table 4, the highest hardness was obtained by water cooling (591±9.4 VHN for sample 1B and 597±15.6 VHN for 2B), and the lowest obtained by open-air cooling (193±10.2 VHN for sample 1D and 217±16.5 for sample 2D). The hardness increased significantly as the cooling rate increased and corresponded to the microstructure result, where samples 1B and 2B have a lath martensite structure. The samples using air media cooling are dominated by pearlite and ferrite. Martensite is a tough constitution due to the carbon trapped in solid solution during fast-cooling. This result tren is similar to Ali et al. result. The hardness of martensite ranges from 635 to 570 HV, and the hardness of bainite mixture microstructure is lower ~ranging from 543 to 430 HVN [24]. Ferrite is being softer phase will affect lower hardness.

Besides that, with the same cooling media, the hardness result of a 75-ton load is slightly higher than 50-ton. It is caused by grain refinement as a result of microstructure in Figure 2 and Figure 3. Smaller grain size causes hardness to increase. During the forging process, the samples undergo a plastic deformation and change their geometry and internal properties due to applying compressive force [25]. Plastic deformation generates residual stress when the load exceeds the elastic limit materials. An increase in the forging load resulted in large surface roughness, compressive residual stress, downward displacement, average height change and outer diameter change [26][27].

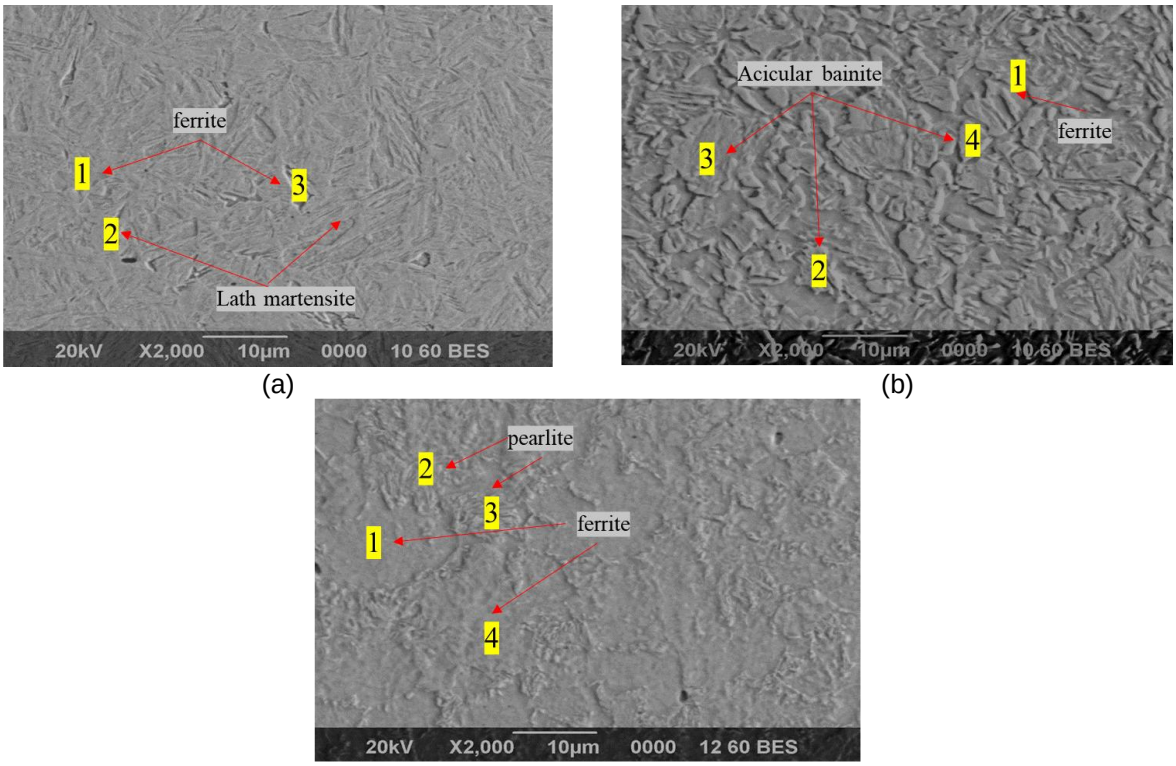

Figure 4. SEM Micrograph of A588-1%Ni after 75-ton forged and heat treatment with (a) water, (b) oil, and (c) open-air cooling

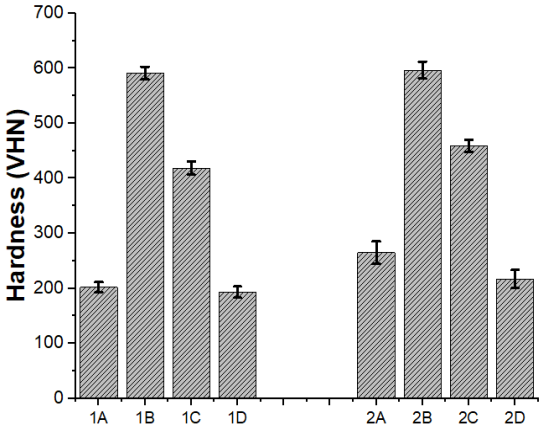

Figure 5. The hardness of A588-1%Ni after hot forging and followed by intercritical heating.

Table 3. EDX-SEM of A588-1% (morphology in Figure 4)

Sample		Cr	Fe	Mn	Ni
Water cooling	1	0.90	99.10	0.90	-
	2	0.82	98.23	0.89	-
	3	0.85	98.22	0.93	-
	4	0.72	99.28	-	-
Oil Cooling	1	0.83	100	-	
	2	0.84	97.54	-	1.62
	3	0.82	100	-	-
	4	0.85	99.15	-	-
Open-air cooling	1	0.77	99.23	-	-
	2	0.79	99.21	-	-
	3	0.87	98.56	0.57	-
	4	0.92	99.08	-	-

Table 4. Correlation between Microstructure and Hardness of A588-1%Ni

Code	Micro-structure	1 (50-ton)	2 (75-ton)
A	Ferrite-pearlite	201.86 ± 9.43	264.74 ± 20.45
B	Martensite-ferrite	591.16 ± 11.80	596.74 ± 15.57
C	Bainite-ferrite	418.58 ± 11.99	459.22 ± 10.62
D	Pearlite-ferrite	193.04 ±10.19	216.9 ± 16.47

Corrosion Analysis of Laterite Steel A588-1%Ni

Corrosion behavior of laterite steel subjected to the forging process and followed by heat treatment was evaluated in 3% NaCl solution. The sample was first immersed for 60 minutes in a 3% NaCl solution with a pH of 6-7 at room temperature, then continued with the Tafel test. The open-circuit potential (OCP) and Tafel polarization curves are shown in Figure 6 and Figure 7. The microstructure has a significant influence on the corrosion behavior of laterite steel.

Figure 6 shows the OCP curve of A588-1%Ni steel after forging and heat treatment. All samples that followed the heat treatment process (sample codes 1B-D and 2B-D) had more negative potentials than those without heat treatment (Samples 1A and 2A), although the difference was insignificant. The range of values of the OCP curve is shown in Table 5. After 1 hour of immersion, the samples without heat treatment (1A and 2A) reached an OCP of about -456.6 mV for a 50-ton load and -465.3 mV vs SCE for loading 75 tons. The distribution of ferrite with a phase containing Fe_3C plays an important role in the initiation and mechanism of corrosion [26][28]. In the 2D sample, there is an increase in the potential value towards the more positive after 3000 s. It allows the formation of a protective layer formed between the pearlite-ferrite phase in a bainite network. The layer is located on the surface of the samples.

In detail, the corrosion behavior can be further determined by the anodic-cathode polarization curve, which is shown in Figure 7.

Table 5. OCP parameter of A588-1%Ni

Sampel	*Open Circuit Potential* (mV vs SCE)	
	Min	Max
1A	-580.3	-456.6
1B	-555.9	-442.7
1C	-537.7	-431.6
1D	-571.9	-506.4
2A	-564.2	-465.3
2B	-541.6	-459.4
2C	-538.6	-401.5
2D	-559.9	-471.3

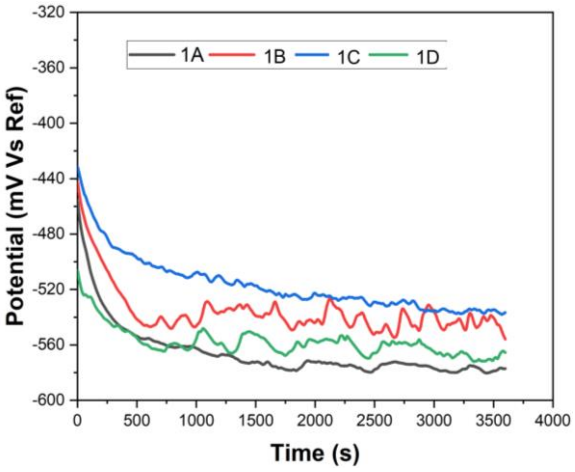

(a)

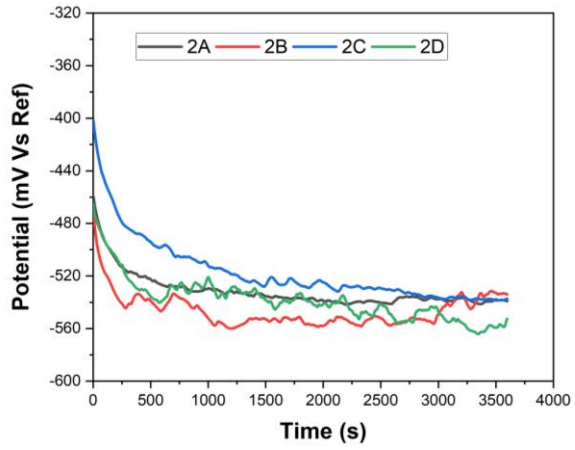

(b)

Figure 6. OCP Curve of A588-1%Ni after hot forging (a) 50 ton (b) 75 ton

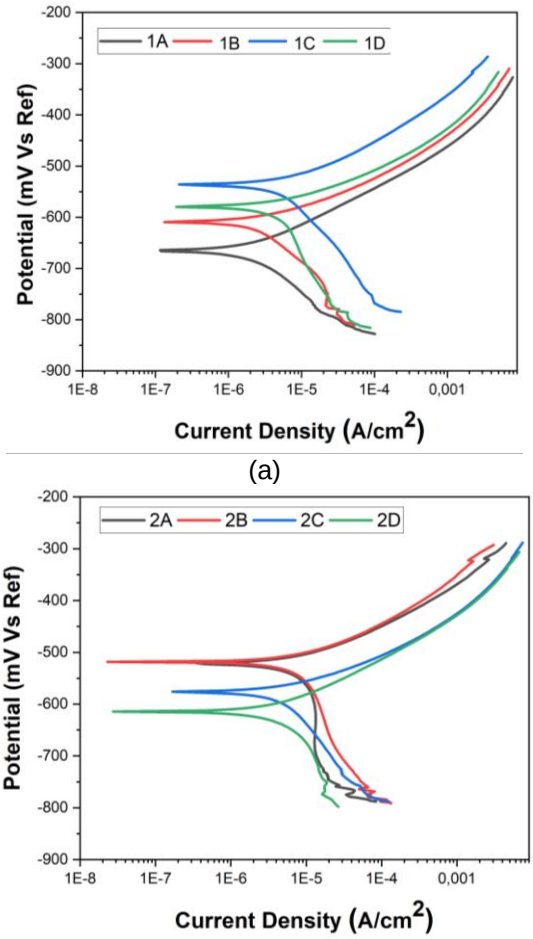

Figure 7. Polarization curve of A588-1%Ni after (a) 50 ton (b) 75-ton hot forging and followed by heat treatment

Figure 7a shows a polarization curve with 50 tons, while Figure 7b shows a polarization curve with a load of 75 tons. Based on Figure 7a, A588-1%Ni laterite steel, after hot forging 50 tons without heat treatment, has the lowest Ecorr corrosion potential (-676.8 mV) and the highest corrosion current density (11.74 x 10^{-6} A/cm²). Adding the heat treatment process shifts the curve to the top right. It is shown that the heat treatment provides a more positive corrosion potential, and the corrosion current density is getting smaller, which means the corrosion rate is getting smaller.

Figure 7b, with a loading of 75 tons, shows a different pattern compared to a loading of 50 tons. The addition of heat treatment after 75 tons of forging will shift the polarization curve to the lower left. It shows that the heat treatment provides a more negative corrosion potential, but the corrosion current density is getting smaller, resulting in a lower corrosion rate. The interpretation of the polarization curve is shown in Table 6.

Table 6. Corrosion parameter

Sample	Beta (10^{-3} V/decade)	Corrosion Potential (mV)	Current Density (10^{-6} A/cm²)	Corrosion Rate (10^{-3} mmpy)
1A	71,51	-676,8	11,74	150,5
1B	129,0	-615,6	2,923	37,45
1C	86,18	-611,8	0,933	11,96
1D	262,0	-579,9	4,360	55,86
2A	413,5	-516,8	8,229	105,4
2B	381,4	-508,3	8,523	109,2
2C	185,5	-561,9	3,799	48,67
2D	162,7	-612,3	4,204	53,86

In general, the forging loads and heat treatment variation greatly affect the corrosion rate of A588-1%Ni laterite steel. Hot forging with a load of 75 tons (samples 2A, 2B, 2C, and 2D) has a higher corrosion rate than 50 tons (samples 1A, 1B, 1C, and 1D). The highest corrosion rates were obtained by non-heat treatment, which were $150.5x10^{-3}$ mmpy and $105.4x10^{-3}$ mmpy. Heat treatment addition can decrease a corrosion rate according to the positivity of corrosion potential and the lower current density, as shown in Figure 7.

The order of corrosion rate is sample 1A>1D>1B>1C for loading 50 tons and 2B 2A>2D>2C for loading 75 tons. Oil cooling with bainite-ferrite microstructure has the lowest corrosion rate, namely $11.96x10^{-3}$ mmpy (1C sample) and 48.67 $x10^{-3}$ mmpy (2C sample). The lowest corrosion rate sample is obtained from the lower current density indicated by the polarization curve (Figure 7a for 1C sample and 7b for 2C sample) getting shifted to the right.

Thus, it concluded that the order of corrosion rate correlates with the resulting microstructure, namely PF (pearlite-ferrite) > MF (martensite-ferrite) > BF (bainite ferrite) or PF MF > BF. The micro-galvanic couple of pearlite-ferrite (PF) and Martensite-ferrite islands accelerate corrosion propagation. The spatial distribution of bainite is more homogeneous than pearlite. Therefore, bainite shows less electrochemical activity and tends to form a dense rust layer with small cracks [11].

The pearlitic is possible for micro-corrosion since cementite is a cathode and ferrite is the anode. Lamellar Fe_3C would be left on the surface, which would accelerate the dissolution of ferrite and tend to a local concentration of Fe^{2+} at the initial stage of corrosion [23]. Fe_3C in the martensitic acts as the cathode and has a negative anchoring effect on the corrosion products, leading to local corrosion.

In addition, grain refinement causes the grain size to get smaller and the grain boundary area to increase. Higher energy and chemical activity than grain boundaries and higher density than this boundary will increase surface reactivity through increased electron activity and diffusion so that Icorr increases more rapidly [28, 29, 30, 31] In addition, the shape and distribution of Fe_3C in bainite, martensite, and pearlite phases also affect the cathodic polarization reaction, which correlates with the oxygen reduction reaction ($O_2 + 2H_2O + 4e = 4OH^-$). However, it is very difficult to determine the pattern of corrosion behavior in the multiphase/dual phase [10].

CONCLUSION

The phase transformations during heating include converting the initial microstructure (ferrite and pearlite) to austenite. In addition, the 75-ton loading tends to have a smaller ferrite grain size when compared to the 50-ton loading. Thus, the greater the forging load, the smaller the grain size formed. The forging process with a load of 50 tons reduced 18±2%, and a load of 75 tons resulted in a percent reduction of 31±1%. Rapid cooling rates (aqueous medium or exceeding 10 °C/s) tend to produce martensite lath, while fairly fast cooling rates (oil media) allow the transformation of lower bainite or martensite to larger/coarse sizes. Heat treatment with air (otherwise known as normalizing) forms microstructures in polygonal ferrite, lamellar pearlite, and lower bainite granular network. The absence of martensite lath due to the slow cooling rate allows sufficient time for the austenite to transform to pearlite. Forging loads and heat treatment also affect the corrosion rate of A588-1%Ni laterite steel in a marine environment. In 3% NaCl corrosion, pearlite has a higher corrosion rate and is more harmful than bainite and martensite. Lamellar Fe_3C in the pearlite phase would accelerate the dissolution of ferrite and tend to a local concentration of Fe^{2+} at the initial stage of corrosion. While Fe_3C in martensitic promotes local corrosion, causes high dislocation energy and breakdown of the corrosion products. The corrosion rates of the steel increase in the following sequence: perlite-ferrite (PF) > martensite-ferrite (MF) > Bainite-ferrite (BF). The highest corrosion rate is a result of air cooling, and the lowest corrosion rate is from oil cooling.

ACKNOWLEDGMENT

This research supported DIPA 2019 from Research Center for Metallurgy and Materials-LIPI. In addition, we thank our colleagues from “Baja Unggul” Research Group, who provided insight and expertise that greatly assisted the research.

REFERENCES

[1] J. Jia, X. Cheng, X. Yang, X. Li, and W. Li, “A study for corrosion behavior of a new-type weathering steel used in harsh marine environment,” *Construction and Building Materials*, vol. 259, p. 119760, 2020, doi: 10.1016/j.conbuildmat.2020.119760.

[2] B. Phull, “2.18 Marine Corrosion,” in *Shreir’s Corrosion*, 2010, pp. 1107–1148.

[3] K. Zakowski, M. Narozny, M. Szocinski, and K. Darowicki, “Influence of water salinity on corrosion risk - The case of the southern

Baltic Sea coast," *Environmental Monitoring and Assessment*, vol. 186, no. 8, pp. 4871–4879, 2014, doi: 10.1007/s10661-014-3744-3.

[4] M. Morcillo, I. Díaz, H. Cano, B. Chico, and D. de la Fuente, "Atmospheric corrosion of weathering steels. Overview for engineers. Part I: Basic concepts," *Construction and Building Materials*, vol. 213, pp. 723–737, 2019, doi: 10.1016/j.conbuildmat.2019.03.334.

[5] ASTM International, "Standard Specification for High-Strength Low-Alloy Structural Steel with 50 ksi [345 MPa] Minimum Yield Point to 4–in. [100–mm] Thick1," *ASTM International*, 2001.

[6] NN, "Pengembangan Baja Laterit-Jembatan Menuju Kemandirian," *Pusat Penelitian Metalurgi dan Meterial-LIPI*, 2014.

[7] S. Herbirowo, L. Hakim, and B. Adjiantoro, "Microstructure and mechanical characteristics of hot forged lateritic steels," in *MATEC Web of Conferences*, 2018, vol. 204, pp. 1–6, doi: 10.1051/matecconf/201820405007.

[8] P. Hasbi, M Yunan; Romijarso, Toni; Paristiawan, "Pengaruh Kecepatan Pendinginan Baja Fasa Ganda Fe-Ni Dan Nilai Kekerasan," *Jurnal Teknologi Bahan dan Barang Teknik*, vol. 10, no. 2, pp. 84–91, 2020, doi: 10.37209/jtbbt.

[9] J. Kaur, B. S. Pabla, and S. S. Dhami, "A Review on Field Areas of Research in Forging Process using FEA,", *International Journal of Engineering Research and Technology,* vol. 5, no. 01, pp. 383–393, 2016, doi: 10.17577/ijertv5is010310.

[10] Y. Zhang, F. Huang, Q. Hu, Z. Peng, and J. Liu, "Effect of micro-phase electrochemical activity on the initial corrosion dynamics of weathering steel," *Materials Chemistry and Physics*, vol. 241, 2020, doi: 10.1016/j.matchemphys.2019.122045.

[11] Z. Wang, X. Zhang, L. Cheng, J. Liu, and K. Wu, "Role of inclusion and microstructure on corrosion initiation and propagation of weathering steels in marine environment," *Journal of Materials Research and Technology*, vol. 10, pp. 306–321, 2021, doi: 10.1016/j.jmrt.2020.11.096.

[12] X. Hao, J. Dong, I. I. N. Etim, J. Wei, and W. Ke, "Sustained effect of remaining cementite on the corrosion behavior of ferrite-pearlite steel under the simulated bottom plate environment of cargo oil tank," *Corrosion Science*, vol. 110, pp. 296–304, 2016, doi: 10.1016/j.corsci.2016.04.042.

[13] O. Abedini, M. Behroozi, P. Marashi, E. Ranjbarnodeh, and M. Pouranvari, "Intercritical heat treatment temperature dependence of mechanical properties and corrosion resistance of dual phase steel," *Materials Research*, vol. 22, no. 1, pp. 1–10, 2019, doi: 10.1590/1980-5373-MR-2017-0969.

[14] J. Hu, S. A. Cao, and J. Xie, "EIS study on the corrosion behavior of rusted carbon steel in 3% NaCl solution," *Anti-Corrosion Methods Mater.*, vol. 60, no. 2, pp. 100–105, 2013, doi: 10.1108/00035591311308074.

[15] Y. Shao, C. Liu, Z. Yan, H. Li, and Y. Liu, "Formation mechanism and control methods of acicular ferrite in HSLA steels: A review," *Journal of Materials Science & Technology*, vol. 34, no. 5, pp. 737–744, 2018, doi: 10.1016/j.jmst.2017.11.020.

[16] F. Zhang, Y. Yang, Q. Shan, Z. Li, J. Bi, and R. Zhou, "Microstructure evolution and mechanical properties of 0.4C-Si-Mn-Cr steel during high temperature deformation," *Materials (Basel).*, vol. 13, no. 1, 2020, doi: 10.3390/ma13010172.

[17] H. Zhao, B. P. Wynne, and E. J. Palmiere, "Conditions for the occurrence of acicular ferrite transformation in HSLA steels," *Journal of Materials Science*, vol. 53, no. 5, pp. 3785–3804, 2018, doi: 10.1007/s10853-017-1781-3.

[18] F. Citrawati, R. Dwiwandono, and L. Firmansyah, "The effect of Ni on the formation of bainite in Fe-Ni lateritic steels through semi-continuous cooling method," *International Journal of Technology*, vol. 11, no. 1, pp. 60–70, 2020, doi: 10.14716/ijtech.v11i1.3178.

[19] D. Loder, S. K. Michelic, and C. Bernhard, "Acicular Ferrite Formation and Its Influencing Factors-A Review," *Journal of Materials Science Research*, vol. 6, no. 1, p. 24, 2016, doi: 10.5539/jmsr.v6n1p24.

[20] C. Liu, L. Shi, Y. Liu, C. Li, H. Li, and Q. Guo, "Acicular ferrite formation during isothermal holding in HSLA steel," *Journal of Materials Science*, vol. 51, no. 7, pp. 3555–3563, 2016, doi: 10.1007/s10853-015-9675-8.

[21] X. Yang *et al.*, "Effect of Cooling Rate and Austenite Deformation on Hardness and Microstructure of 960MPa High Strength Steel," *Science and Engineering of Composite Materials*, vol. 27, no. 1, pp. 415–423, 2020, doi: 10.1515/secm-2020-0045.

[22] G. Liang *et al.*, "Effect of cooling rate on microstructure and mechanical properties of a low-carbon low-alloy steel," *Journal of*

Materials Science, vol. 56, no. 5, pp. 3995–4005, 2021, doi: 10.1007/s10853-020-05483-9.

[23] Z. Li, W. Xue, Y. Chen, W. Yu, and K. Xiao, "Microstructure and Grain Boundary Corrosion Mechanism of Pearlitic Material," *Journal of Materials Engineering and Performance*, 2021, doi: 10.1007/s11665-021-06171-8.

[24] M. Ali, D. Porter, J. Kömi, M. Eissa, H. El Faramawy, and T. Mattar, "Effect of cooling rate and composition on microstructure and mechanical properties of ultrahigh-strength steels," *Journal of Iron and Steel Research International.*, vol. 26, no. 12, pp. 1350–1365, 2019, doi: 10.1007/s42243-019-00276-0.

[25] S. Mancini, L. Langellotto, G. Zangari, R. Maccaglia, and A. Di Schino, "Optimization of open die ironing process through artificial neural network for rapid process simulation," *Metals (Basel).*, vol. 10, no. 10, pp. 1–14, 2020, doi: 10.3390/met10101397.

[26] N. Karunathilaka *et al.*, "Effect of lubrication and forging load on surface roughness, residual stress, and deformation of cold forging tools," *Metals (Basel).*, vol. 9, no. 7, 2019, doi: 10.3390/met9070783.

[27] D. Prayitno and M. Irsyad, "Effect of Ratio of Surface Area on the Corrosion Rate," *SINERGI*, vol. 22, no. 1, pp. 13-18, 2018, doi: 10.22441/sinergi.2018.1.002

[28] O. O. and D. K. G. T. N. Guma, "Effects of Some Heat Treatments on Corrosion of Low and Medium Carbon Steel in Acidic Chloride Medium," *World Scientific News*, vol. 132, no. June, pp. 169–186, 2019.

[29] A. Arwati and S. Sianipar, "Corrosion study of SS316L in environment sulphur acid using weight loss method," *SINERGI*, vol. 22, no. 1, pp. 24-28, 2018, doi: 10.22441/sinergi.2018.1.005

[30] Y. P. Asmara, "Simulation of CO2 Corrosion of Carbon Steel in High Pressure and High Temperature Environment (HPHT)," *Journal of Integrated and Advanced Engineering (JIAE)*, vol. 2, no. 1, pp. 63-70, 2022, doi: 10.51662/jiae.v2i1.41

[31] M. Soleimani, H. Mirzadeh, and C. Dehghanian, "Effect of grain size on the corrosion resistance of low carbon steel plate," *Materials Research Express*, vol. 7, p. 016522, 2020, doi: 10.4028/www.scientific.net/msf.984.43.